Parametrization and Application of a Coarse Grained Force Field for Benzene/Fullerene Interactions with Lipids

Russell DeVane,*,† Arben Jusufi,† Wataru Shinoda,‡ Chi-cheng Chiu,§ Steven O. Nielsen,§ Preston B. Moore,# and Michael L. Klein†

Institute for Computational Molecular Science and Department of Chemistry, Temple University, 1901 North 13th Street, Philadelphia, Pennsylvania 19122, United States, RiCS, Nanosytsem Research Institute, National Institute of Advanced Industrial Science and Technology (AIST), Central 2, 1-1-1, Umezono, Tsukuba, Ibaraki 305-8568, Japan, Department of Chemistry, The University of Texas at Dallas, 800 West Campbell Road, Richardson, Texas 75080, United States, and Department of Chemistry & Biochemistry, University of the Sciences in Philadelphia, 600 South 43rd Street, Philadelphia, Pennsylvania 19104, United States

Received: July 27, 2010; Revised Manuscript Received: October 28, 2010

Recently, we reported new coarse grain (CG) force fields for lipids and phenyl/fullerene based molecules. Here, we developed the cross parameters necessary to unite those force fields and then applied the model to investigate the nature of benzene and C_{60} interactions with lipid bilayers. The interaction parameters between the phenyl and lipid CG sites are based on experimental and all atom (AA) molecular dynamics (MD) data. The resulting force field was tested on benzene rich lipid bilayers and shown to reproduce general behavior expected from experiments. The parameters were then applied to C_{60} interactions with lipid bilayers. Overall, the results showed excellent agreement with AA MD and experimental observations. In the C_{60} lipid systems, the fullerenes were shown to aggregate even at the lowest concentrations investigated.

1. Introduction

The complex nature of fullerene behavior in vivo is of great interest due to potential applications in medicine.[1−17] Widespread use of nanomaterials will require a firm understanding of the toxicity posed by these systems.[8−10] Recent studies have indicated that carbon nanospheres can penetrate cell membranes, enter cellular interiors, cross blood−brain barriers, and even enter cellular nuclei.[11,12]

Despite much work, there still exists some confusion regarding the toxicity of C_{60}.[5,13−16] Some experiments have suggested a connection to solubility in water.[14] These experiments have focused on so-called pristine, nano- and derivatized (water-soluble) forms of C_{60}.[14] However, certain results are at odds with these findings, suggesting that more work is needed.[17] One question that remains open is the behavior of fullerenes in lipid membrane systems. Although various studies have indicated active (endocytosis) and passive (diffusion) mechanisms for entry into cells, a firm understanding of the nature of fullerene interactions with lipid membrane systems is still of primary importance.[3,18−20]

While the complex interactions occurring between fullerenes and biological machinery in vivo poses a currently insurmountable barrier to theoretical approaches, the subset of interactions occurring between fullerenes and lipid membrane systems is an ideal and manageable target. To this end, computational studies have been performed using model lipid bilayer systems (typically composed of a single biologically relevant lipid type) in place of biological membranes.[21−25] All atom (AA) molecular dynamics (MD) studies have provided insight into the details of these interactions. Li et al. used AA MD simulations to determine that the equilibrium position of a single C_{60} molecule in a dimyristoylphosphatidylcholine (DMPC) lipid bilayer was $\approx$6−7 Å off center in the bilayer core.[21] Further, they determined that the effective interaction between two C_{60} monomers in a DMPC bilayer was less attractive than in an alkane melt with the same molecular weight as the lipid chains. Bedrov et al. calculated the transfer free energy profile of a single C_{60} through a DMPC bilayer showing that the free energy decreases as the fullerene enters the hydrophobic bilayer core with no barrier associated with entry.[22] Other studies investigated the interactions of C_{60} and derivatized C_{60} with a dipalmitoylphosphatidylcholine (DPPC) bilayer including calculation of a PMF for the translocation of the fullerene across the bilayer.[24] Despite these and other contributions, AA MD simulations have been limited by the accessible temporal and spatial scales as a result of computational overhead associated with these calculations. More to the point, the study of aggregation of C_{60} in lipid bilayers has been limited to monomer and dimer based simulations rather than many C_{60} molecules interacting simultaneously.

To circumvent these problems and make more efficient use of current computational resources, an alternative to AA models are the so-called coarse grained (CG) models. With CG MD, a trade-off is made between the high level of detail inherent in AA MD and the computational efficiency brought about by reducing that level of detail. The process involves representing several atoms with a single CG site. A significant increase in the system sizes and simulation time scales results.[27,26] D'Rozario et al. used CG MD to study the interactions of pristine and derivatized C_{60} with DPPC lipid bilayers and found that the level of derivitization had a significant effect on the nature of the interactions with the lipid bilayer.[26] Wong-Ekkabut et al. used the MARTINI CG force field to study the interactions of C_{60} with dioleoylphosphatidylcholine (DOPC) and DPPC lipid

* To whom correspondence should be addressed. E-mail: devane@temple.edu.
† Temple University.
‡ National Institute of Advanced Industrial Science and Technology.
§ The University of Texas at Dallas.
# University of the Sciences in Philadelphia.

10.1021/jp1070264
Published on Web 11/19/2010

bilayers.[25] Their simulations indicate that C_{60} spontaneously enters the lipid bilayer and that no aggregation takes place within the lipid bilayer. Further, they showed that C_{60} clusters easily enter the lipid bilayer but disintegrate once inside.

With the primary intention of studying the interaction of C_{60} with lipid bilayers, we extended our existing CG models to allow the investigation of these systems. To do so, it was necessary to develop interaction parameters to unite our recently developed CG force fields for phenyl based molecules[27,28] and phosphatidylcholine (PC) based lipids.[29] The parameter sets are based on the same model previously developed by our group.[30] The phenyl based force field was shown to be transferable and useful for applications including C_{60} and carbon nanotubes (CNTs).[27,28] The lipid force field parameters were shown to accurately model PC lipid systems including monolayers, bilayers, and vesicles.[29] Combined, the force fields permit the investigation of the interactions occurring between benzene/C_{60} and lipid bilayers.[29] The resulting force field is shown to be highly effective at accurately representing both benzene−lipid and C60−lipid interactions when compared to AA MD and experiment.

The methodology will be presented in section 2. Results will be given in section 3 including details of the parametrization along with applications to benzene-lipid and C_{60}−lipid systems. The current work will be summarized in section 4.

2. Methods

2.1. Coarse Grained Mapping. The CG mapping used in our approach typically places three to four heavy atoms per CG site.[27−30] For phenyl based molecules the resolution was increased to better maintain the planar nature of the phenyl based molecules as was discussed in our previous work.[27] This increased resolution maps 1.5 heavy atoms per CG site for benzene (the 6 carbons in benzene are represented by 4 spherical noncharged CG sites). For comparison, in the case of toluene and xylene, this mapping resolution decreases to 1.75 heavy atoms per CG site and 2 heavy atoms per CG site, respectively. The benzene based CG site (labeled BER) was selected to model fullerenes.[29] On the basis of the CG:AA carbon mapping ratio of 2:3 from the CG benzene model, a CG C_{60} molecule should contain 40 interaction sites. The arrangement of these 40 CG sites to model C_{60} was discussed in our previous work.[28] The fullerene molecule was treated as a rigid body in the MD studies using the rigid module in LAMMPS; the use of a rigid body description precludes bond and angle potentials.[31]

2.2. Molecular Dynamics Simulation. All AA MD simulations performed here were carried out using the CHARMM PARAM27 force field parameters[32] in the NAMD[33] or GROMACS 4[34] simulation packages. Note that for DOPC lipid simulations in GROMACS, a conversion must be applied according to Siu et al.[35] For all simulations, periodic boundary conditions were used in all three Cartesian directions.

For NAMD simulations, bonds involving hydrogen atoms were constrained via the SHAKE/RATTLE method.[36] A 2 fs time step was used to integrate the equations of motion. Nonbonded interactions were cutoff at 12 Å. The long-range Coulomb interactions were calculated via the particle mesh Ewald method with a grid spacing of approximately 1.0 Å.[37,38]

For GROMACS simulations, all bonds involving hydrogen atoms were constrained by using the LINCS[39] and the SETTLE[40] (for water hydrogens) algorithms allowing a time step of 2 fs. Nonbonded interactions were cutoff at 10 Å. Long-range electrostatic interactions were treated using the particle-mesh Ewald method[37,38] with a grid spacing of 1.2 Å with cubic interpolation between the grid points. Using a Berendsen thermostat the system was coupled to a temperature bath with a coupling constant of 1 ps^{-1} .

The DMPC lipid bilayer simulations employed a constant area ensemble (NP_nAT with x and y directions fixed) with an area of 60.6 $Å^2$/lipid molecule. As recently discussed in detail,[35] the DOPC systems require constant surface tension to ensure a realistic area per lipid of around 72.0 $Å^2$.[35,41] The surface tension was maintained at 44 mN/m (22 mN/m per interface) while the pressure perpendicular to the bilayer surface (z direction) was kept at 1 bar using Berendsen pressure coupling with a relaxation time of 1 ps and a water compressibility of 4.5×10^{-5} bar^{-1}. Simulations were run at 298 and 310 K for DOPC and DMPC, respectively.

CG MD simulations were performed using the LAMMPS MD package from the Sandia National Laboratory.[31] All CG simulations were carried out using a two level RESPA multitime step integrator.[42] The bond and angle potentials were evaluated with the inner time step of 2 fs, and the nonbonded interactions were evaluated with the outer time step of 10 fs. The temperature and the pressure were controlled using the Nosé-Hoover algorithm.[43] Nonbonded interactions were cutoff at 10 Å and electrostatics (including long ranged interactions) were calculated using the LAMMPS implementation of the particle−particle particle-mesh method with a grid spacing of 2.0 Å. The CG water model was taken from the CG force field developed by Shinoda et al.[30] The interactions involving the BER site used the parameters we recently developed.[27,28] CG lipid parameters were taken from our recently developed model for PC lipids.[29] For all simulations, visualization and analysis was performed using the VMD visualization tool.[44]

2.3. Free Energy Calculation. The free energy methods used for the AA MD calculations will be discussed first followed by the methodology for the CG MD calculations. The AA MD free energy calculations were performed using umbrella sampling. A benzene/fullerene (solute) molecule was initially placed in the water region approximately 20 Å from the interface in a fully hydrated DOPC or DMPC lipid bilayer system. The z-component (the bilayer normal) of the separation between the solute center and the membrane center of mass was fixed and is denoted as z_0. Lateral mobility of the solute was allowed at each separation z_0. Distance constraints were enforced by applying an umbrella harmonic spring potential with a force constant of 24 kcal/(mol·$Å^2$). Initially, the system was equilibrated for 50 ns. Thereafter, the solute was successively moved in the z-direction to the bilayer center plane in 1.0 Å steps. At each separation window, the system was equilibrated for 20 ns followed by a 10 ns production run. The step size was decreased to 0.5 Å and the run times increased in regions where the slope of the PMF varied considerably, such as in the headgroup regions. The recorded force histograms were combined using the weighted histogram analysis method (WHAM)[45] through its numerical implementation by Grossfield (http://membrane.urmc.rochester.edu). Systems contained 128 lipids total with roughly 6200 waters for both DMPC and DOPC.

For the CG MD calculations of the transfer free energy, steered MD simulations were carried out using the LAMMPS MD package.[31] Equilibrated fully hydrated DOPC and DMPC bilayer systems were used as initial configurations. A single solute molecule was placed in the water region of the system and pulled into the center of the bilayer using a constant velocity pulling speed of 1 Å/ns and a force constant of 100 kcal/(mol·$Å^2$). Multiple pulls (≈50) were performed for each system for a total simulation time of 1.2 μs per system. Equivalent

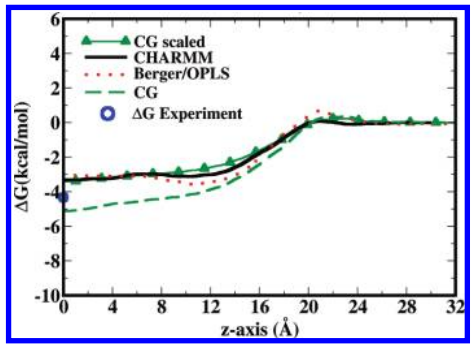

Figure 1. Free energy profile for the translocation of benzene from a reference state in bulk water to the center (0.0 Å) of a DOPC lipid bilayer. The Berger-OPLS[49] result is shown as the dotted line, the CHARMM result is shown as the solid line, and the CG result is plotted with a dashed line. To aid in comparison, the CG result is also scaled by 1/1.5 and shown as a solid line marked with triangles. The experimental value for ΔG from Simon et al. is shown (circle) for comparison.[50]

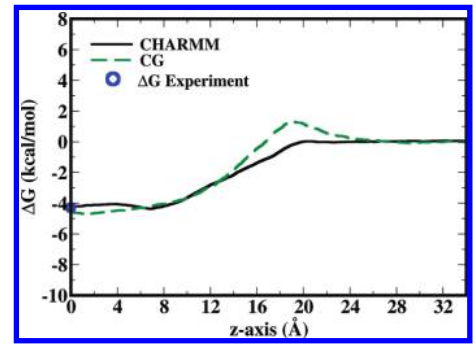

Figure 2. Free energy profile for the translocation of benzene from a reference state in bulk water to the center (0.0 Å) of a DMPC bilayer. The results from the CHARMM AA MD calculation (solid line) are compared to the results from the CG MD calculation (dashed line). The experimental value for ΔG from Simon et al. is shown (circle) for comparison.[50]

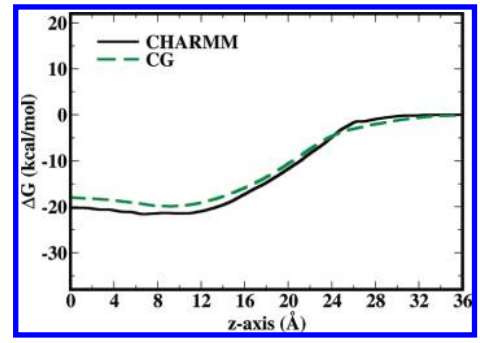

Figure 3. Free energy profile for the translocation of C_{60} from a reference state in bulk water to the center (0.0 Å) of a DOPC bilayer. The plot compares results from the CHARMM AA MD calculation (solid line) and the CG MD calculation (dashed line).

system sizes were used for the CG MD simulations as given for the AA MD calculation above.

3. Results and Discussion

3.1. Partitioning in Lipid Bilayers. To fix and validate the BER−lipid interactions, comparison to AA MD calculations was necessary. The BER−alkane (CM, three carbon alkane segment not at the chain terminus; CT, three carbon alkane segment at the alkane chain terminus; CT2, two carbon alkane segment at the alkane chain terminus) interactions were previously fixed using water/alkane partitioning data.[27,28] The remaining parameters to be fixed consisted of the BER-lipid headgroup (NC, choline; PH, phosphate; GL, glycerol; EST, ester) interactions and BER-unsaturated alkane (CMD2) interactions. The BER-CMD2 interaction is needed for the DOPC lipid systems (see Figure 1 of Shinoda et al.[29] for CG lipid mapping). To set these parameters, AA MD transfer free energy calculations were performed for benzene in DMPC and DOPC and C_{60} in DOPC. The nonbonded parameters fit here were ε and σ from the Lennard-Jones functional form given in eq 1.

$$v(r)_{9-6} = \frac{27}{4}\varepsilon\left(\frac{\sigma^9}{r^9} - \frac{\sigma^6}{r^6}\right) \tag{1}$$

The details of the force field were discussed in our previous work.[27] For parametrization, the Lorentz−Berthelot combining rules (eq 2) were used.

$$\sigma_{ab} = \frac{\sigma_{aa} + \sigma_{bb}}{2} \qquad \varepsilon_{ab} = \sqrt{\varepsilon_{aa}\varepsilon_{bb}} \tag{2}$$

In eq 2, ε_{aa} and σ_{aa} represent the self-interaction values for species "a" and ε_{ab} and σ_{ab} represent those for the cross interactions between species "a" and "b". Using eq 2, we made a first guess for σ and ε. With σ held fixed, ε was adjusted to give the best agreement for the three transfer free energy calculations.

This simultaneous fitting of the BER-lipid interactions for all systems gave the results shown in Figure 1−3. Figure 1 shows the AA MD and CG MD results for the transfer free energy of benzene from water to the center (0.0 Å) of a fully hydrated DOPC bilayer. The dotted line shows results previously published using the Berger lipid and OPLS force field[46−49] and the solid line shows our calculation using the CHARMM force field.[32] The CG result is shown as the dashed line and a reported experimental value of $\Delta G = -4.34$ kcal/mol is shown marked with a circle on the y-axis.[50] The calculated values for Berger, CHARMM and the CG model are −3.1, −3.4, and −5.1 kcal/mol, respectively. The CG model shows very good agreement with the experimental value.

Discrepancy between the AA MD and CG MD results could arise from the fact that the alkane interactions in the CG model were fit to volume corrected water−alkane transfer free energy data.[27] Experiments indicate that organic phase-water partition coefficients of benzene into nonpolar isotropic liquids, micelles, and unilamellar lipid vesicles all agreed to within 7% of each other.[50−52] This is the case for the CG model where the water to alkane and the water to lipid bilayer transfer free energies agree very well. On the other hand, the AA MD models more closely reproduce nonvolume corrected transfer free energy. Again, for the AA MD simulations, the water to alkane (cyclohexane) and water to lipid transfer free energies are very similar, which was previously discussed.[49]

Another aspect to compare is the shape of the free energy profile especially in the alkane region. To aid in comparison, the CG result was divided by 1.5 and is shown marked with triangles in Figure 1. This factor was chosen to scale the magnitude of the CG result to match that from the CHARMM result. With this scaling, it is easier to compare the relative shapes of the AA and CG profiles. The results show that none of the models predict a high level of localization of benzene in a specific region of the hydrophobic chains but rather suggest that the benzene is distributed throughout the hydrophobic

TABLE 1: Nonbonded Parameters Developed for the Interaction between the CG Lipid Sites and CG Phenyl Site[a]

types	ε (kcal/mol)	σ (Å)
BER-NC	0.1987	4.775
BER-PH	0.3997	4.600
BER-GL	0.2711	4.153
BER-EST	0.2240	4.050
BER-CMD2	0.1768	3.9025

[a] CG types are taken from our previous work. BER refers to the phenyl CG site,[27] NC, PH, GL, and EST are from the lipid head-group, and CMD2 refers to the unsaturated alkane section from the lipid tail group.[29] The interactions are based on the Lennard-Jones 9-6 nonbonded potential form (eq 1) with a 15.0 Å cutoff.[27] Note that σ is based on the mixing rules given in eq 2. A full database of parameters in a LAMMPS input style is given in the Supporting Information.

region. The Berger result shows a slightly deeper well around the headgroup/alkane interface compared to the CHARMM result. This is even less evident in the CG model. However, the difference between the CHARMM result and the CG (scaled) result is minor (compare solid line to triangles).

Figure 2 shows the results for the transfer free energy of benzene from water to the center (0.0 Å) of a fully hydrated DMPC bilayer. The CHARMM AA MD result is shown by the solid line and the CG result is shown by the dashed line. Here, the models demonstrate excellent agreement ($\Delta G_{AA} = -4.3$ and $\Delta G_{CG} = -4.7$ kcal/mol) compared to one another and compared to a reported experimental result of −4.30 kcal/mol (circle on y-axis).[50] The results also agree well with previous AA MD results published using free energy methodology.[53] Again, both profiles suggest that benzene is distributed throughout the hydrophobic region of the lipid bilayer. The CG model shows a slightly larger barrier to entry into the bilayer compared to the AA result. However, this must be considered in light of the DOPC result shown above where the barriers to entry agree well. Since the same headgroup parameters exist in the DMPC and DOPC CG models (and in the AA model), a compromise must be made.

Figure 3 shows the free energy of transferring C_{60} from water to the center (0.0 Å) of a DOPC bilayer from CHARMM AA (solid) and CG (dashed) MD calculations. This CG result was based on the same parameters used for the benzene calculations above. The CG model shows excellent agreement with the AA results, indicating a high level of transferability of the CG model. The transfer free energy, ΔG, was −21.5 and −19.5 kcal/mol for AA and CG, respectively. In this case, neither the AA nor the CG model predicts a barrier to entry into the bilayer.

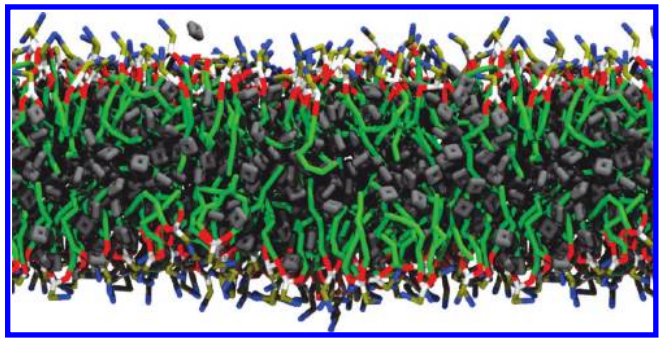

Figure 4. Snapshot of the high concentration benzene−DOPC system. The alkane chains are shown in green, the EST groups are shown in red, the GL groups are shown in white, the PH groups are shown in gold, and the NC groups are blue. The benzenes are gray. Water was removed for clarity.

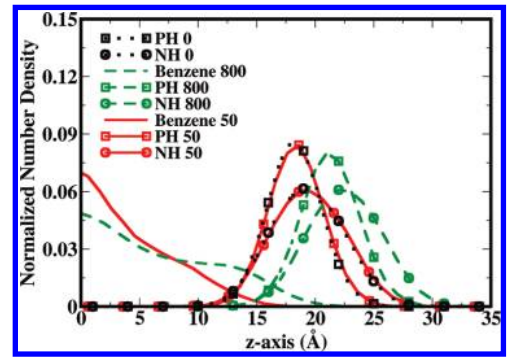

Figure 5. Profile taken along the z-axis (normal to the membrane bilayer) for the benzene−DOPC system. The normalized number densities for the lipid headgroup, NC (circles) and PH (squares), and benzene (no symbol) are shown for the pure lipid system (dotted), the 50 benzene system (solid), and the 800 benzene system (dashed). Note that the total density integrates to one in all cases.

TABLE 2: Area per Lipid Molecule and the Lipid Bilayer Thickness for the Benzene−DOPC and C_{60}−DOPC Systems

no. of benzene/fullerene molecules	area/lipid (Å^2)	lipid bilayer thickness (Å)
0	68	40
50 benzene	70	41
800 benzene	90	45
32 C_{60}	68	40
98 C_{60}	69	41
200 C_{60}	70	41

The results shown here represent the outcome of a simultaneous fitting of the three systems (benzene in DOPC and DMPC and fullerene in DOPC) along with the constraint that the BER−alkane interactions were previously fit to reproduce the water−alkane transfer free energy.[27,28] It is noted that the BER−CMD2 (CMD2 makes up part of the hydrophobic tail group in our CG DOPC model) interaction was fit to give good agreement for the benzene and fullerene DOPC systems. The resulting BER-CMD2 parameters are consistent with those previously determined for the alkanes using transfer free energy calculations.[27] The parameters developed here are tabulated in Table 1. A full set of parameters for a solvated C_{60}−DOPC system in a LAMMPS input style is given in the Supporting Information. The model indicates a high level of transferability in that the parameters are capable of accurately modeling benzene and C_{60}. It should be noted that the atomistic simula-

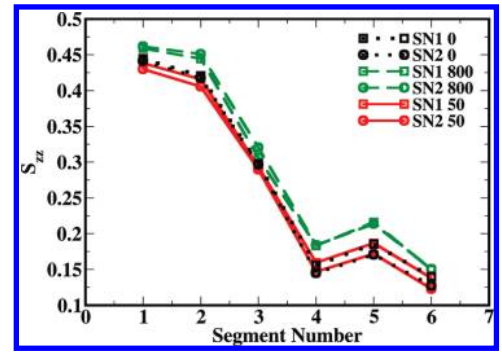

Figure 6. CG order parameters for the benzene−DOPC lipid systems calculated along the bonds (vectors) connecting the CG sites. The measurements were taken along each chain from the EST group to the terminal alkane CG site. The angle was taken relative to the z-axis (membrane normal). The pure lipid, 50 benzene, and 800 benzene systems are shown with dotted, solid, and dashed lines, respectively. Both alkane chains, SN1 (square) and SN2 (circles), are shown.

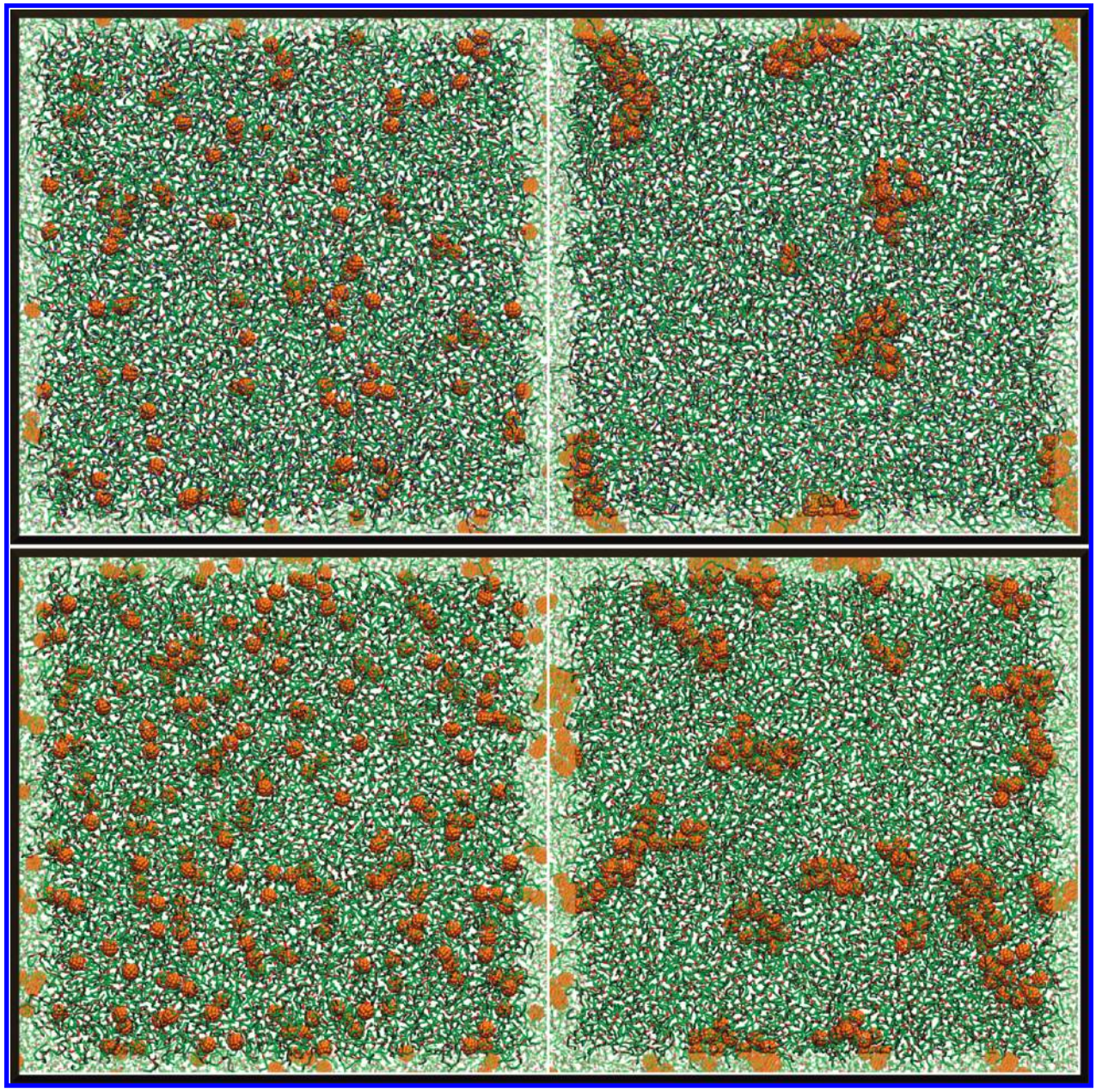

Figure 7. Snapshots from above the bilayer for the initial and final configurations of the DOPC C_{60} simulations containing 98 fullerenes (upper) and 200 fullerenes (lower) are shown here. In each panel, the left snapshot shows the initial (after all of the C_{60} has been steered into the bilayer) configuration and the right snapshot shows the final configuration. The lipid colors are the same as those used in 4. Here, C_{60} is orange. The edges of the periodic images are shown with a transparent representation to aid in visualization of the clusters that cross the simulation unit cell.

tions within CHARMM use different parameters to represent benzene and C_{60}.[22,23] If more detail is required, the BER CG type could be split into two separate CG types and refined to model benzene and fullerenes independently as in the CHARMM case. However, we feel the performance is more than acceptable and choose not to pursue this approach.

3.2. Benzene Rich Lipid Bilayers. As an application of the parameters developed here, the impact of benzene on a DOPC lipid bilayer was investigated for various benzene concentrations. Two systems composed of a DOPC bilayer (200 lipid molecules total) and 4296 CG waters combined with 50 benzenes and 800 benzenes were used, resulting in a benzene:lipid ratio of 1:4 and 4:1, respectively. The simulations were carried out for 50 ns. Several simulation based studies on the interactions of benzene with lipid bilayers have been carried out in the past.[49,54−59] Figure 4 shows a snapshot from the end of the higher concentration benzene simulation. The behavior of the benzene and its impact on the bilayer was observed to be concentration dependent, as shown by earlier studies.[50,60,61]

Figure 5 shows the normalized number density profiles along the normal to the membrane interface for the pure DOPC bilayer (dotted line), the lower concentration (solid line) and the higher concentration (dashed line) systems. Shown are the headgroup profiles for the NC (circles) and PH (squares) CG sites and benzene (no symbol). From this figure, it is seen that for the lower benzene concentration system, no significant impact was made on the density profile of the headgroups. Further, the benzene is distributed throughout the hydrophobic region of the bilayer. Table 2 shows that the area per molecule increased only slightly from 68 $Å^2$ for the pure lipid system to 70 $Å^2$ while the bilayer thickness remained constant at 38 Å. The area per molecule was calculated by taking the area of the bilayer (product of the x and y dimensions of the simulation cell) from the simulations (where the pressure was allowed to fluctuate

anisotropically) and dividing by the number of lipid molecules in a single leaflet of the bilayer.

Order parameters were measured using eq 3,

$$S_{zz} = \frac{1}{2}\langle 3\cos^2\theta - 1\rangle \quad (3)$$

where θ is the angle between the vectors created by the bonds connecting the CG sites and the z-axis. Measurements were made in the lipid molecules beginning at the EST site and continuing to the terminal alkane CG site. Comparison was made between the benzene containing systems and the pure lipid system for the SN1 (squares) and SN2 (circles) chains, as shown in Figure 6. Here the results indicate that there is no significant difference in this property when the lower benzene concentration system (solid line) is compared to the pure lipid system (dotted line).

On the other hand, the higher benzene concentration (4:1) leads to significant changes in the bilayer structure. The dashed line in Figure 5 shows a significant shift of the headgroup density profiles out of the membrane, indicating swelling of the bilayer. Table 2 shows that the area per molecule increased to 90 Å^2 while the lipid bilayer showed an increase in thickness to 45 Å, which was also seen in the density profile. Figure 6 shows the order parameters for the higher concentration system (dashed line) where an increase in ordering along the entire length of both chains can be seen. Finally, the presence of free monomers in the aqueous phase, as seen in Figure 4, suggests that this concentration is close to the saturation point.

3.3. C_{60} Aggregation in Lipid Bilayers. To investigate the behavior of C_{60} in a lipid bilayer, simulations of varying fullerene concentration were performed using the parameters developed here. Three simulations of 32, 98, and 200 C_{60} molecules in a DOPC bilayer composed of 2048 DOPC lipids and 68 064 CG waters were performed. These concentrations correspond to DOPC:C_{60} ratios of 64:1, 21:1, and 10:1, respectively. The total system sizes contained roughly 110 000 CG sites (corresponding to roughly 1 million atoms) and were carried out for simulation times ranging from 130 to 330 ns. Figure 7 shows snapshots from above the bilayer for the 98 and 200 fullerene molecule simulations. Simulations of this size and time scale are not practical with an AA MD approach and rely on methods such as CG MD for exploration. In addition to the systems containing fullerenes, a reference simulation free of fullerene but otherwise identical was carried out. Our simulations indicated that C_{60} spontaneously enters the bilayer, which has been found in other simulation studies.[24−26] However, to cut down on the computational expense of allowing multiple fullerenes to diffuse into the bilayer interior from the water region, a steering force was applied over the first 1 ns of the simulation to drive the fullerenes into the bilayer core. The steering force was then removed. This protocol was used on all three systems.

For the 32 fullerene system, the fullerenes started to aggregate immediately and continued to build larger clusters as the simulation proceeded. The average aggregation number (2 for this system) as a function of simulation time is shown in the upper plot of Figure 8 (circles). The aggregation number plateaus for this system because the low concentration leads to diffusion limited aggregation. The upper-middle plot of Figure 8 shows the distribution of aggregate sizes for the last frame of the 32 fullerene system which is characterized by several free monomers and smaller aggregates along with roughly three larger aggregates (of 5 monomers or larger). Figure 9 shows the

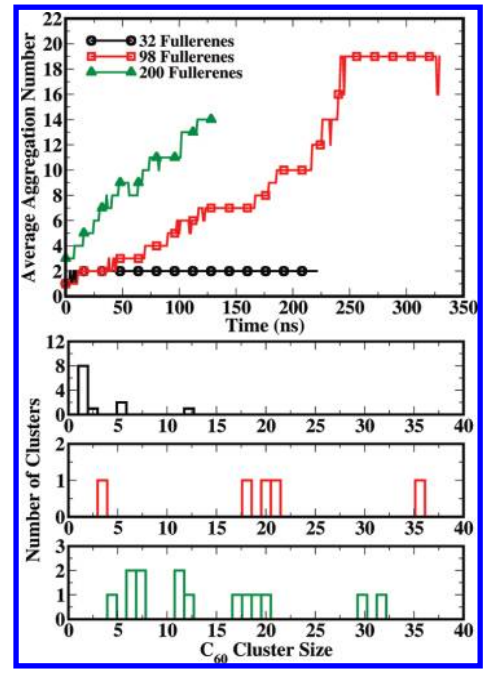

Figure 8. Aggregation results are shown here for the C_{60}−DOPC systems. The upper panel shows the time evolution of the average aggregation number for the 32 fullerene (circles), 98 fullerene (squares), and 200 fullerene (triangles) systems. The lower three panels show the distribution of aggregate sizes from the last snapshot of the three systems with the 32 fullerene system shown in the upper plot, 98 fullerene system shown in the middle, and 200 fullerene system in the lower plot.

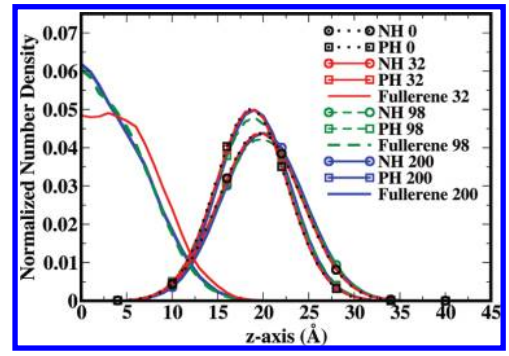

Figure 9. Normalized number density profiles along the z-axis (normal to the membrane bilayer) for the C_{60}−DOPC system are shown here. The headgroups and fullerene densities are shown for the pure lipid system (black), the 32 fullerene system (red), 98 fullerene system (green), and 200 fullerene system (blue). The NC groups (circles), PH groups (squares), and C_{60} (no symbol) are shown. Note that the total density integrates to one in each case.

normalized number density profiles for the headgroups, NC (circles) and PH (squares), and the fullerene (no symbols) along the bilayer interface normal. In this figure, the pure lipid and 32 fullerene systems are shown in black and red, respectively. The density profiles indicate that the 32 fullerene system lipid structure is not impacted relative to the pure lipid system. Further, the CG order parameters in Figure 10 show no significant differences for the pure lipid (black) and the 32 fullerene system (red).

The upper panel of Figure 7 shows snapshots from the 98 fullerene system for the initial configuration (after all of the C_{60} is in the bilayer) on the left and the final configuration (after 330 ns) on the right. The fullerenes quickly began to aggregate in the core of the bilayer. Due to the longer simulation time, the aggregates grew to sizes of roughly 20 monomers on

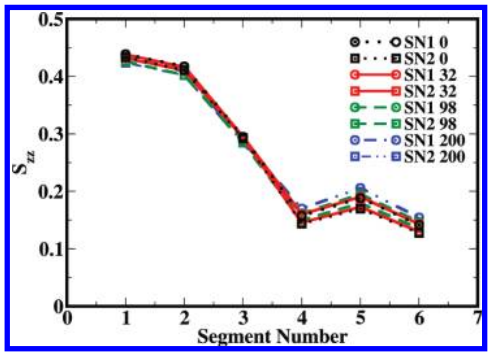

Figure 10. CG order parameters for the C_{60}−DOPC systems calculated along the bonds (vectors) connecting the CG sites. The measurements were taken along each chain from the EST group to the terminal alkane CG site in the lipid alkane chains. The angle was taken relative to the *z*-axis (membrane normal). The pure lipid system is shown in black, the 32 fullerene system is shown in red, the 98 fullerene system is shown in green, and the 200 fullerene system is shown in blue. The two chains, SN1 and SN2, are marked with circles and squares, respectively.

average. The distribution of aggregate sizes is shown in the lower middle plot of Figure 8 where an aggregate of considerable size (35 molecules) can be seen in addition to smaller aggregates. As shown in Table 2, no significant impact was made on the area per molecule of the lipid or the bilayer thickness. This indicates the degree to which the alkane region of the bilayer can be compressed without affecting the packing of the headgroups. The density profile in Figure 9 shows no perturbation of the bilayer headgroups, and the fullerenes were distributed throughout the bilayer hydrophobic core but with an elevated tendency to occupy the center of the bilayer. The order parameters show a very minor increase in Figure 10.

The lower panel of Figure 7 shows the snapshots for the 200 fullerene system with the initial configuration on the left and the final snapshot after 130 ns on the right. Over the course of the simulation, large aggregates formed and appeared to be continuing to form albeit retarded by the slow diffusion rates of the relatively large aggregates. Figure 11 shows a side view from the end of the 200 fullerene simulation. Here, the aggregates can be clearly seen. Further, no significant impact on the lipid bilayer (in the form of induced curvature or similar distortions) is visibly detectable. The time evolution of the average aggregate size is shown in the upper panel of Figure 8 marked by triangles. The lower panel shows the aggregate size distribution at the end of the simulation.

The results shown here indicate that C_{60} forms aggregates in a DOPC bilayer even at the lowest concentration investigated. These observations are in agreement with a number of experimental observations.[62−66] Work on charge transport across a DPPC lipid bilayer containing C_{70} fullerenes yielded transit times of the negative charge that suggests an electronic process as opposed to diffusion of charge across the bilayer.[63] These findings could be explained by the existence of C_{70} aggregates that rapidly and efficiently transport charge across the bilayer. For C_{60} containing DPPC lipid bilayer systems, small angle neutron scattering (SANS), X-ray reflectivity and grazing incident small-angle X-ray scattering (GISAXS) studies were used to investigate the effects of fullerene.[65] This work indicated perturbations of the bilayer thickness and suggested the presence of C_{60} aggregates. The lack of perturbations in the current CG simulations more than likely results from the relatively small aggregates that have formed compared to those in the experimental work. The results shown in Figure 8 do not indicate the final aggregation numbers. It is expected that the aggregates would grow larger with longer simulation times and perhaps more importantly larger concentrations of C_{60}. Finally, work on the formation and dispersion of C_{60} in DPPC bilayers indicated the formation of nano-C_{60} aggregates in lipid bilayer systems with ratios of DOPC:C_{60} of 500:1.[66]

On the other hand, these results are in contrast to the work by Wong-Ekkabut et al. where the use of the MARTINI model predicted fullerene dispersion in a DOPC bilayer.[25] The concentrations investigated in those simulations (DOPC:C_{60} 72:1, 18:1, and 9:1) and the system size (1152 DOPC molecules) were on the order of those used here. These discrepancies reflect differences in the models. More work and experimental guidance will be required to resolve these differences.

4. Conclusions

In this work, we developed parameters for the interactions between our recently developed CG benzene (fullerene) force field and CG lipid force field. This parametrization was based on a combination of experimental data and AA MD calculations. The results showed excellent agreement for three distinct systems (benzene in DOPC and DMPC bilayers and C_{60} in a DOPC bilayer) when compared to AA MD transfer free energy calculations of solute molecules from water into lipid bilayers. This is an indication of a high level of transferability of the CG models. The parameters were then used to investigate the impact of benzene and fullerene on lipid bilayer systems.

The results indicate that a high concentration of benzene can be obtained before significant effects to a DOPC bilayer are observed. With the system containing 1 benzene to 4 lipids, no significant effects were noted on the lipid bilayer. However, at a benzene:lipid ratio of 4:1, significant effects were observed. At all concentrations, the benzene is distributed throughout the hydrophobic core of the bilayer with an increase in density toward the center of the bilayer. The benzene does not aggregate but rather remains diffuse throughout the bilayer even at the highest concentration. Further, the presence of occasional free

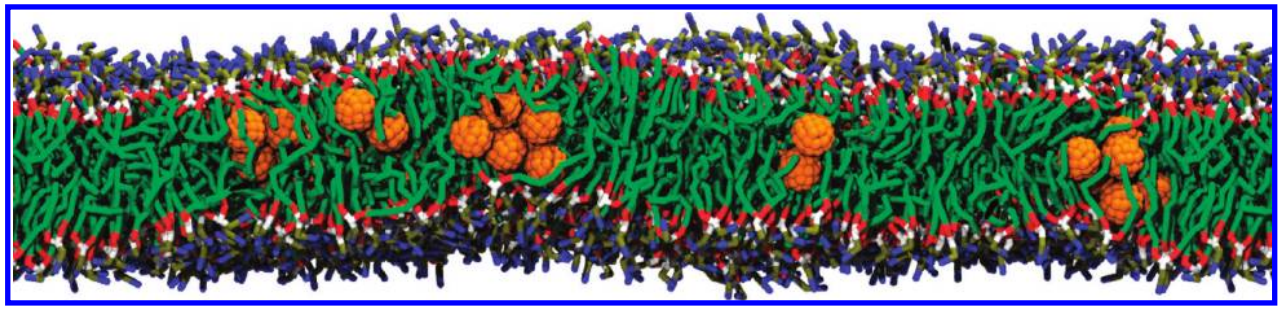

Figure 11. Side view from the final configuration of the C_{60}−DOPC simulation containing 200 fullerenes. The lipid colors are the same as those used in 4. Here, C_{60} is orange.

monomers in the aqueous phase indicates that the highest concentration is near the saturation point.

The primary result reported here is the behavior of multiple fullerenes in a lipid bilayer. In earlier work, our CG MD model indicated a favorable dimerization free energy for C_{60} in a tridecane melt[28] which was in excellent agreement with previous AA MD simulations by Li et al.[21] On the other hand, the AA MD simulations from Li et al. found a less favorable free energy for the dimerization of C_{60} in a DMPC lipid bilayer.[21] On the basis of this result, Li et al. postulated an increased solubility of fullerenes in the lipid bilayer interior (compared to a hydrocarbon melt).[21] In line with this postulate, Wong-Ekkabut et al. observed complete dispersal of C_{60} in a DOPC lipid bilayer using the MARTINI CG force field.[26] Despite long simulation times, no C_{60} aggregation was noted. In fact, aggregates in the aqueous phase were shown to disintegrate upon entry into the bilayer in those simulations.

The results from this work indicate that C_{60} aggregates within a DOPC bilayer at all concentrations investigated. From an initially dispersive state, the fullerenes aggregate rapidly with the aggregates continuing to grow in size despite being increasingly limited by the diffusion time scale. It appears that the aggregates are still growing at the end of the simulations. These findings are supported by several experiments, which clearly show evidence for C_{60} aggregation in lipid bilayers.[62−66]

The validation of the CG force field developed here is promising for the application to more advanced systems involving the interactions of fullerenes with lipids. In addition, the results indicate that the CG model is transferable which opens up a realm of possible applications including different sized fullerene spheres (C_{180}, C_{540}), carbon nanotubes and derivatized fullerenes including carboxylated C_{60} and CNTs.

Acknowledgment. M.L.K., R.D., and A.J. thank the National Science Foundation for support of this research. This research was also supported in part by the National Science Foundation through TeraGrid resources provided by ORNL under grant number TG-MCA93S020. W.S. is grateful for the support of the Next Generation Super Computing Project, Nanoscience Program, MEXT, Japan. S.O.N. acknowledges support from the SRC/SEMATECH Engineering Research Center for Environmentally Benign Semiconductor Manufacturing.

Supporting Information Available: Full set of parameters for a solvated C_{60}−DOPC system in a LAMMPS input style. This material is available free of charge via the Internet at http://pubs.acs.org.

References and Notes

(1) Dugan, L.; Lovett, E.; Quick, K.; Lotharius, J.; Lin, T.; O'Malley, K. *Parkinsonism Relat. D* **2001**, *7*, 243–246.
(2) Gonzalez, K.; Wilson, L.; Wu, W.; Nancollas, G. *Bioorg. Med. Chem.* **2002**, *10*, 1991–1997.
(3) Pantarotto, D.; Singh, R.; McCarthy, D.; Erhardt, M.; Briand, J.; Prato, M.; Kostarelos, K.; Bianco, A. *Angew. Chem. Int. Ed.* **2004**, *43*, 5242–5246.
(4) Kam, N.; Dai, H. *J. Am. Chem. Soc.* **2005**, *127*, 6021–6026.
(5) Gharbi, N.; Pressac, M.; Hadchouel, M.; Szwarc, H.; Wilson, S.; Moussa, F. *Nano Lett.* **2005**, *5*, 2578–2585.
(6) Sayes, C.; Liang, F.; Hudson, J.; Mendez, J.; Guo, W.; Beach, J.; Moore, V.; Doyle, C.; West, J.; Billups, W.; Ausman, K.; Colvin, V. *Toxicol. Lett.* **2006**, *161*, 135–142.
(7) Liu, Z.; Tabakman, S.; Welsher, K.; Dai, H. *Nano Res.* **2009**, *2*, 85–120.
(8) Maynard, A. D.; Aitken, R. J.; Butz, T.; Colvin, V.; Donaldson, K.; Oberdoerster, G.; Philbert, M. A.; Ryan, J.; Seaton, A.; Stone, V.; Tinkle, S. S.; Tran, L.; Walker, N. J.; Warheit, D. B. *Nature* **2006**, *444*, 267–269.
(9) Nel, A.; Xia, T.; Madler, L.; Li, N. *Science* **2006**, *311*, 622–627.
(10) Oberdoerster, G.; Stone, V.; Donaldson, K. *Nanotoxicology* **2007**, *1*, 2–25.
(11) Oberdorster, E. *Environ. Health Persp.* **2004**, *112*, 1058–1062.
(12) Selvi, B. R.; Jagadeesan, D.; Suma, B. S.; Nagashankar, G.; Arif, M.; Balasubramanyam, K.; Eswaramoorthy, M.; Kundu, T. K. *Nano Lett.* **2008**, *8*, 3182–3188.
(13) Andrievsky, G.; Klochkov, V.; Derevyanchenko, L. *Fullerenes, Nanotubes, Carbon Nanostruct.* **2005**, *13*, 363–376.
(14) Sayes, C.; Fortner, J.; Guo, W.; Lyon, D.; Boyd, A.; Ausman, K.; Tao, Y.; Sitharaman, B.; Wilson, L.; Hughes, J.; West, J.; Colvin, V. *Nano Lett.* **2004**, *4*, 1881–1887.
(15) Sayes, C.; Gobin, A.; Ausman, K.; Mendez, J.; West, J.; Colvin, V. *Biomaterials* **2005**, *26*, 7587–7595.
(16) Mori, T.; Takada, H.; Ito, S.; Matsubayashi, K.; Miwa, N.; Sawaguchi, T. *Toxicology* **2006**, *225*, 48–54.
(17) Sayes, C. M.; Marchione, A. A.; Reed, K. L.; Warheit, D. B. *Nano Lett.* **2007**, *7*, 2399–2406.
(18) Kam, N.; Jessop, T.; Wender, P.; Dai, H. *J. Am. Chem. Soc.* **2004**, *126*, 6850–6851.
(19) Lu, Q.; Moore, J.; Huang, G.; Mount, A.; Rao, A.; Larcom, L.; Ke, P. *Nano Lett.* **2004**, *4*, 2473–2477.
(20) Li, W.; et al. *Nanotechnology* **2008**, *19*, 145102.
(21) Li, L.; Davande, H.; Bedrov, D.; Smith, G. D. *J. Phys. Chem. B* **2007**, *111*, 4067–4072.
(22) Bedrov, D.; Smith, G. D.; Davande, H.; Li, L. *J. Phys. Chem. B* **2008**, *112*, 2078–2084.
(23) Li, L.; Bedrov, D.; Smith, G. *Phys. Rev. E* **2005**, *71*, 011502.
(24) Qiao, R.; Roberts, A. P.; Mount, A. S.; Klaine, S. J.; Ke, P. C. *Nano Lett.* **2007**, *7*, 614–619.
(25) Wong-Ekkabut, J.; Baoukina, S.; Triampo, W.; Tang, I.-M.; Tieleman, D. P.; Monticelli, L. *Nat. Nanotechnol.* **2008**, *3*, 363–368.
(26) D'Rozario, R. S. G.; Wee, C. L.; Wallace, E. J.; Sansom, M. S. P. *Nanotechnology* **2009**, *20*, 115102.
(27) DeVane, R.; Klein, M. L.; Chiu, C.; Nielsen, S. O.; Shinoda, W.; Moore, P. B. *J. Phys. Chem. B* **2010**, *114*, 6386–6393.
(28) Chiu, C.; DeVane, R. H.; Klein, M. L.; Shinoda, W.; Moore, P. B.; Nielsen, S. O. *J. Phys. Chem. B* **2010**, *114*, 6394–6400.
(29) Shinoda, W.; DeVane, R. H.; Klein, M. L. *J. Phys. Chem. B* **2010**, *114*, 6836–6849.
(30) Shinoda, W.; DeVane, R. H.; Klein, M. L. *Mol. Simul.* **2007**, *33*, 27–36.
(31) Plimpton, S. *J. Comput. Phys.* **1995**, *117*, 1–19.
(32) MacKerell, A.; et al. *J. Phys. Chem. B* **1998**, *102*, 3586–3616.
(33) Phillips, J.; Braun, R.; Wang, W.; Gumbart, J.; Tajkhorshid, E.; Villa, E.; Chipot, C.; Skeel, R.; Kale, L.; Schulten, K. *J. Comput. Chem.* **2005**, *26*, 1781–1802.
(34) Hess, B.; Kutzner, C.; van der Spoel, D.; Lindahl, E. *J. Chem. Theory Comput.* **2008**, *4*, 435–447.
(35) Siu, S. W. I.; Vacha, R.; Jungwirth, P.; Boeckmann, R. A. *J. Chem. Phys.* **2008**, *128*, 125103.
(36) Martyna, G.; Tuckerman, M.; Tobias, D.; Klein, M. L. *Mol. Phys.* **1996**, *87*, 1117–1157.
(37) Darden, T.; York, D.; Pedersen, L. *J. Chem. Phys.* **1993**, *98*, 10089–10092.
(38) Essmann, U.; Perera, L.; Berkowitz, M.; Darden, T.; Lee, H.; Pedersen, L. *J. Chem. Phys.* **1995**, *103*, 8577–8593.
(39) Hess, B.; Bekker, H.; Berendsen, H.; Fraaije, J. *J. Comput. Chem.* **1997**, *18*, 1463–1472.
(40) Miyamoto, S.; Kollman, P. *J. Comput. Chem.* **1992**, *13*, 952–962.
(41) Liu, Y.; Nagle, J. *Phys. Rev. E* **2004**, *69*, 040901.
(42) Tuckerman, M.; Berne, B.; Martyna, G. *J. Chem. Phys.* **1991**, *94*, 6811–6815.
(43) Hoover, W. *Phys. Rev. A* **1985**, *31*, 1695–1697.
(44) Humphrey, W.; Dalke, A.; Schulten, K. *J. Mol. Graphics* **1996**, *14*, 33.
(45) Kumar, S.; Bouzida, D.; Swendsen, R.; Kollman, P.; Rosenberg, J. *J. Comput. Chem.* **1992**, *13*, 1011–1021.
(46) Berger, O.; Edholm, O.; Jahnig, F. *Biophys. J.* **1997**, *72*, 2002–2013.
(47) Jorgensen, W.; Maxwell, D.; TiradoRives, J. *J. Am. Chem. Soc.* **1996**, *118*, 11225–11236.
(48) Kaminski, G.; Friesner, R.; Tirado-Rives, J.; Jorgensen, W. *J. Phys. Chem. B* **2001**, *105*, 6474–6487.
(49) MacCallum, J. L.; Bennett, W. F. D.; Tieleman, D. P. *Biophys. J.* **2008**, *94*, 3393–3404.
(50) Simon, S.; McDaniel, R.; McIntosh, T. *J. Phys. Chem.* **1982**, *86*, 1449–1456.
(51) McDaniel, R.; Simon, S.; McIntosh, T.; Borovyagin, V. *Biochemistry* **1982**, *21*, 4116–4126.
(52) Sikkema, J.; de Bont, J.; Poolman, B. *J. Biol. Chem.* **1994**, *269*, 8022–8028.
(53) Matubayasi, N.; Shinoda, W.; Nakahara, M. *J. Chem. Phys.* **2008**, *128*, 195107.

(54) Bassolinoklimas, D.; Alper, H.; Stouch, T. *Biochemistry* **1993**, *32*, 12624–12637.
(55) Tieleman, D. P.; Marrink, S.; Berendsen, H. *Biochim. Biophys. Acta* **1997**, *1331*, 235–270.
(56) Norman, K. E.; Nymeyer, H. *Biophys. J.* **2006**, *91*, 2046–2054.
(57) Bemporad, D.; Luttmann, C.; Essex, J. W. *Biophys. J.* **2004**, *87*, 1–13.
(58) Bemporad, D.; Essex, J. W.; Luttmann, C. *J. Phys. Chem. B* **2004**, *108*, 4875–4884.
(59) Orsi, M.; Sanderson, W. E.; Essex, J. W. *J. Phys. Chem. B* **2009**, *113*, 12019–12029.
(60) DeYoung, L.; Dill, K. *Biochemistry* **1988**, *27*, 5281–5289.
(61) Tu, K.; Tarek, M.; Klein, M. L.; Scharf, D. *Biophys. J.* **1998**, *75*, 2123–2134.
(62) Hungerbuhler, H.; Guldi, D.; Asmus, K. *J. Am. Chem. Soc.* **1993**, *115*, 3386–3387.
(63) Niu, S.; Manzerall, D. *J. Am. Chem. Soc.* **1996**, *118*, 5791–5795.
(64) Janot, J.; Bienvenue, E.; Seta, P.; Bensasson, R.; Tome, A.; Enes, R.; Cavaleiro, J.; Leach, S.; Camps, X.; Hirsch, A. *J. Chem. Soc., Perkin Trans. 2* **2000**, 301–306.
(65) Jeng, U.; Hsu, C.; Lin, T.; Wu, C.; Chen, H.; Tai, L.; Hwang, K. *Physica B* **2005**, *357*, 193–198.
(66) Chen, Y.; Bothun, G. D. *Langmuir* **2009**, *25*, 4875–4879.

JP1070264